07

Functional signal transformer based on a composite multiferroic

© L.M. Krutyansky, V.L. Preobrazhensky

Prokhorov Institute of General Physics, Russian Academy of Sciences, Moscow, Russia
E-mail: leonid.krut@kapella.gpi.ru

Received April 14, 2023
Revised May 10, 2023
Accepted June 2, 2023

Nonlinear transfer functions of a voltage converter realized in a straintronic composite magnetic–piezoelectric structure within the area of spin reorientation (SR) are studied numerically and analytically. It is shown that at the SR critical point the transfer function has the shape of an inverse sigmoid. As the magnetizing field strength decreases, the function transforms into a reversible hysteresis loop. Under a pulsed impact, the threshold effect of generation of an opposite-polarity spike is displayed, which is followed by the system return to its initial state. When the input represents a sequence of short pulses critical with respect to the time of impact, the system switches between bistable spin states with inversion of the output voltage polarity. The qualitatively different functions of nonlinear voltage transform can be performed in one and the same structure by controlling the magnetic field strength and input signals' parameters.

Keywords: magnetic–piezoelectric structure, transfer function, nonlinearity, threshold switching.

DOI: 10.61011/TPL.2023.08.56683.19594

Functional signal transformers serve as elements of analog computing systems, program control systems, and automatic and extreme control systems. During last years, the interest in nonlinear functional transformations has increased significantly because of advancement in analog neuromorphic networks. Typical neuromorphic elements combine the functions of weighted summation of input signals with nonlinear transformation of the summed signal [1]. The nonlinear transformation can involve the function of a threshold element generating a response to an exceedance of the preset impact parameters. To perform neural-like signal transformations with the aid of electronic components, different physical principles and techniques are used, which are described, for instance, in review [2]. In some cases, approaches developed earlier for the Random-Access-Memory (RAM) systems [3–6] are being adapted to the problem of neuromorphic networks. One of the promising physical principles of the RAM implementation, which is characterized by ultralow power consumption, is based on the magnetoelectric interaction in solid-state structures. During last years, a significant progress has been achieved in the field of creating composite straintronic magnetoelectric structures piezoelectric–magnetic in which the magnetoelectric coupling is induced by simultaneous deformation of the piezoelectric and magnetostrictive components [7–9]. The magnetoelectric interaction is most efficiently realized under the conditions of spin-reorientation (SR) transitions in the magnetic system [10–12]. A background for considering a straintronic structure as a functional signal converter was the proposed and deeply developed fully magnetoelectric read-and-write circuit [9,13]. Provided the memory systems do not impose special requirements for the functional coupling of the write and read signals, the transfer function is the main characteristic of signal transformers.

In this work there were studied the transfer functions of the piezoelectric–magnetic–dielectric composite structure whose magnetic subsystem undergoes the SR transition. The structure's schematic view is presented in Fig. 1, *a*. As a piezoelectric we consider a $\langle 011 \rangle$ crystal of $Pb(Mg_{1/3}Nb_{2/3})O_3-PbTiO_3$ (PMN–PT) with the size of $4 \times 4 \times 0.3$ mm in the x, y, z directions, respectively; under appication of normal electric field, the crystal undergoes anisotropic strain in the xy plane. As a material for magnetic layers, there was considered an intermetallic heterostructure $TbCo_2$/FeCo 150 μm thick with a uniaxial magnetic anisotropy being induced during the fabrication [8]. The spin system of rare-earth compound $TbCo_2$ ensures giant magnetostriction $\lambda_S \approx 10^{-4}$. The exchange coupling of the $TbCo_2$ and FeCo layers causes general ferromagnetic ordering of the structure. The magnetic field application in the structure plane perpendicular to the easy-magnetization axis (EA) provides conditions for the SR transition. The magnetic layers are able not only to perform the function of nonlinear signal transformation but also to play the role of electrodes for detecting output voltage V_{out}. The dielectric layer 5 μm thick provides decoupling of input voltages and weighted summing of input signals for the multi-electrode excitation system which simulates the functions of dendrites in neuromorphic elements. In this case, the top magnetic electrode simulates the axon function. The dielectric parameters were assumed to be the same as those of TiO_2. Since the total charge at the input electrodes is equal in magnitude to the opposite-sign charge at the piezoelectric top cladding, the input voltage is defined as $V_{in} = \sum_i V_i c_i / \sum_i c_i$, where V_i is the voltage at the i-th electrode, and c_i is the partial capacity between the electrode and top cladding.

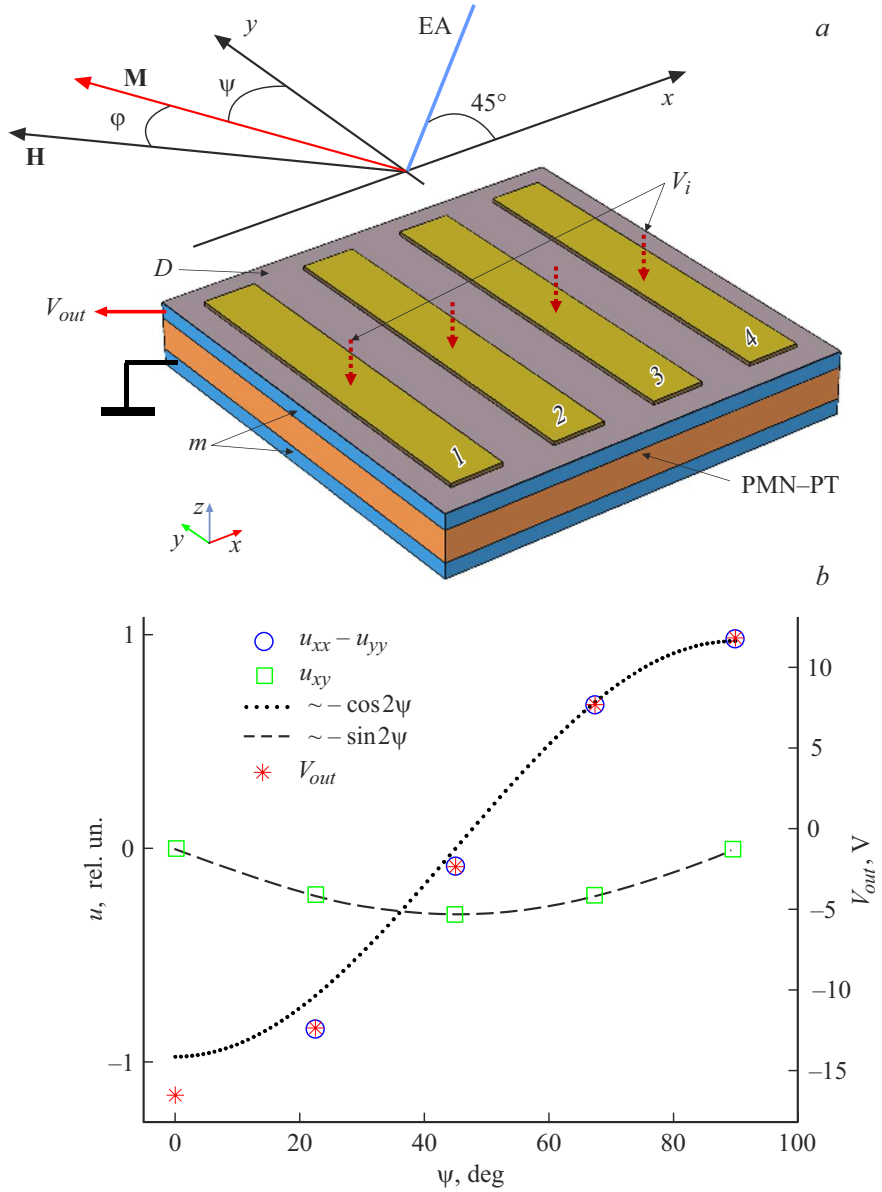

Figure 1. *a* — schematic view of the composite structure. PMN–PT — piezoelectric layer, *m* — magnetostrictive layers, *D* — dielectric layer, *1–4* — input electrodes, V_i — potentials at the input electrodes, V_{out} — output voltage. The vector diagram indicates directions of the easy-magnetization axis (EA), magnetic moment **M**, and magnetizing field **H**. *b* — calculations of the orientation-angle dependences of strains and output voltage of the piezoelectric.

Nonlinear transfer functions relating the structure output voltage to the input voltage get formed as a result of elastic interaction of the magnetic and piezoelectric subsystems. In the approximation of isotropic magnetostriction characterized by constant B, the magneto-elastic energy is defined as

$$F_{me} = -B\sin 2\varphi(u_{xx} - u_{yy}) - 2B\cos 2\varphi u_{xy}, \qquad (1)$$

where u_{ij} are the strain tensor components, φ is the deflection angle between the magnetization and the magnetic field (see Fig. 1, *a*). The magnetic system of layers with an effective field of uniaxial magnetic anisotropy H_A is described by constitutive equation

$$\frac{H}{H_A}\sin\varphi - \frac{1}{2}\sin 2\varphi - \frac{2B}{MH_A} \times \left[(u_{xx} - u_{yy})\cos 2\varphi - 2u_{xy}\sin 2\varphi\right] = 0. \qquad (2)$$

The piezoelectric part of the ⟨011⟩ PMN–PT crystal in the normally oriented electric field **E** is

$$F_p = -E_3(e_{31}u_{xx} + e_{32}u_{yy} + e_{33}u_{zz}), \qquad (3)$$

where e_{ij} are the piezoelectric modules. Notice that modules e_{31} and e_{32} in PMN–PT have opposite signs,

which ensures in-plane piezo-strain anisotropy necessary for coupling the piezoelectric and magnetic subsystems.

Linearity of the elasticity equations allows independent calculation of the piezo-effect and magnetostriction contributions to the strain. Fig. 1, *b* presents the calculated dependence of strains averaged over the magnetic volume on the magnetization direction. The simulation was carried out by using the COMSOL Multiphysics code. Parameters of the materials were taken from [14–17]. The function of summing the input signals was demonstrated via calculation of output voltages (5.15, 10.33, 15.52 and 20.67 V) for the case of applying voltage of 25 V to the input electrodes from one to four, respectively.

Taking into account the contribution of voltage at the piezoelectric V_{out}, the following relations were obtained for the strains:

$$\langle u_{xx} - u_{yy} \rangle - g_p V_{out} + g_m^{(1)} \sin 2\varphi,$$

$$\langle u_{xy} \rangle = g_m^{(2)} \cos 2\varphi, \qquad (4)$$

where

$$g_p = -0.07 \cdot 10^{-5}\,\mathrm{V}^{-1},\ g_m^{(1)} = -10^{-4},\ g_m^{(2)} = -3.1 \cdot 10^{-5}.$$

Voltage V_{out} created by input signal V_{in} and magnetostriction was obtained in the following form:

$$V_{out} = g_V V_{in} + g_m^{(3)} \sin 2\varphi + V_Q, \qquad (5)$$

where $g_m^{(3)} = -14\,\mathrm{V}$, $g_V = 0.78$.

Numerical coefficients in equations (4) and (5) were determined from the calculations presented in Fig. 1, *b*. Parameter V_Q is a ratio between the alternating charge on the piezoelectric top cladding and total capacity of the piezoelectric and dielectric. The charge is caused by the finite leakage resistance in the dielectric and piezoelectric layer. Accounting for the leakage resistances is necessary to determine the magnetic system equilibrium state in the absence of input signal. The charge relaxation equation is

$$\frac{\partial P}{\partial t} = -\frac{1}{\tau}\left(P - \kappa \sin 2\varphi\right) - U_{in}\left(\frac{1}{\tau} - \frac{1}{\tau_1}\right), \qquad (6)$$

where dimensionless variables are $P = 2V_Q g_p B/MH_A$, $U_{in} = 2V_{in} g_p g_V B/MH_A$, $\kappa = -2g_p g_m^{(3)} B/MH_A$, while τ and τ_1 are the charge relaxation times in the piezoelectric and dielectric layers, respectively. In further calculations, relation $2B/MH_A = -3 \cdot 10^3$ was used. In the same variables $U_{out} = 2V_{out} g_p B/MH_A$ and equation (2) gets transformed to

$$\frac{H}{H_A}\sin\varphi - \frac{1}{2}\sin 2\varphi = \left[P + U_{in} - (\kappa + \eta)\sin 2\varphi\right]\cos 2\varphi, \qquad (7)$$

where $\eta = -\left(g_m^{(1)} - 2g_m^{(2)}\right)2B/MH_A$.

The results of simultaneous solution of equations (5)–(7) are presented in Figs. 2, 3. In further analysis of the solutions, by the input and output voltages are assumed to be dimensionless quantities U_{in} and U_{out}. When

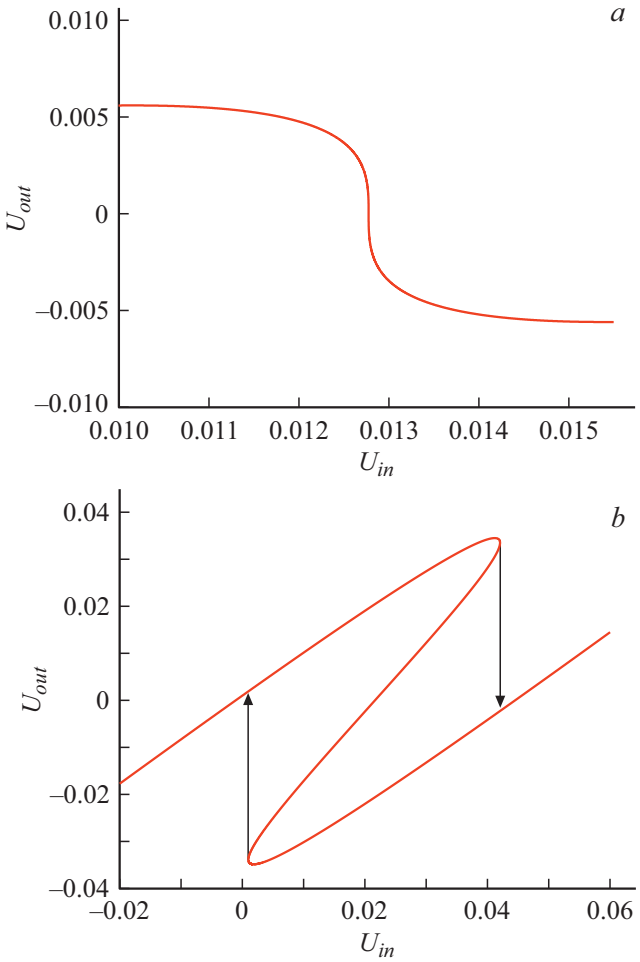

Figure 2. Transfer functions of the structure at two magnetizing fields and respective equilibrium orientation angles of the magnetic moment. *a* — $H = 1.18\,H_A$, $\varphi_0 = -0.22$; *b* — $H = 1.05\,H_A$, $\varphi_0 = -0.43$. Arrows indicate the output voltage switch directions.

magnetostriction is ignored, the field strength critical for the SR transition is $H_c = H_A$. According to equation (6), stable equilibrium in the absence of input signal is characterized by equation $P_0 = \kappa \sin 2\varphi_0$ relating the charge at the piezoelectric top cladding to the magnetization direction. Along with this, spontaneous magnetostrictive strains in the structure at $\varphi_0 = 0$ and $\eta \neq 0$ enhance the SR transition critical field to $H_c = 1.24\,H_A$. At the critical point, the spin system susceptibility to piezoelectric's voltage U_{out} increases abnormally, which is typical for second-order phase transitions. However, the spin system remains stable with respect to input signal U_{in} which changes quite rapidly as compared with the charge relaxation rate, while the transfer function becomes cubic.

With abnormally increasing susceptibility, the instability shifts towards weaker fields $H = 1.18\,H_A$, while the equilibrium magnetization deflects from the magnetizing field by angle $\varphi_0 = -0.22$. The transfer function takes the shape of an inverse sigmoid shown in Fig. 2, *a*. Further decrease in the magnetizing field gives rise to a hysteresis

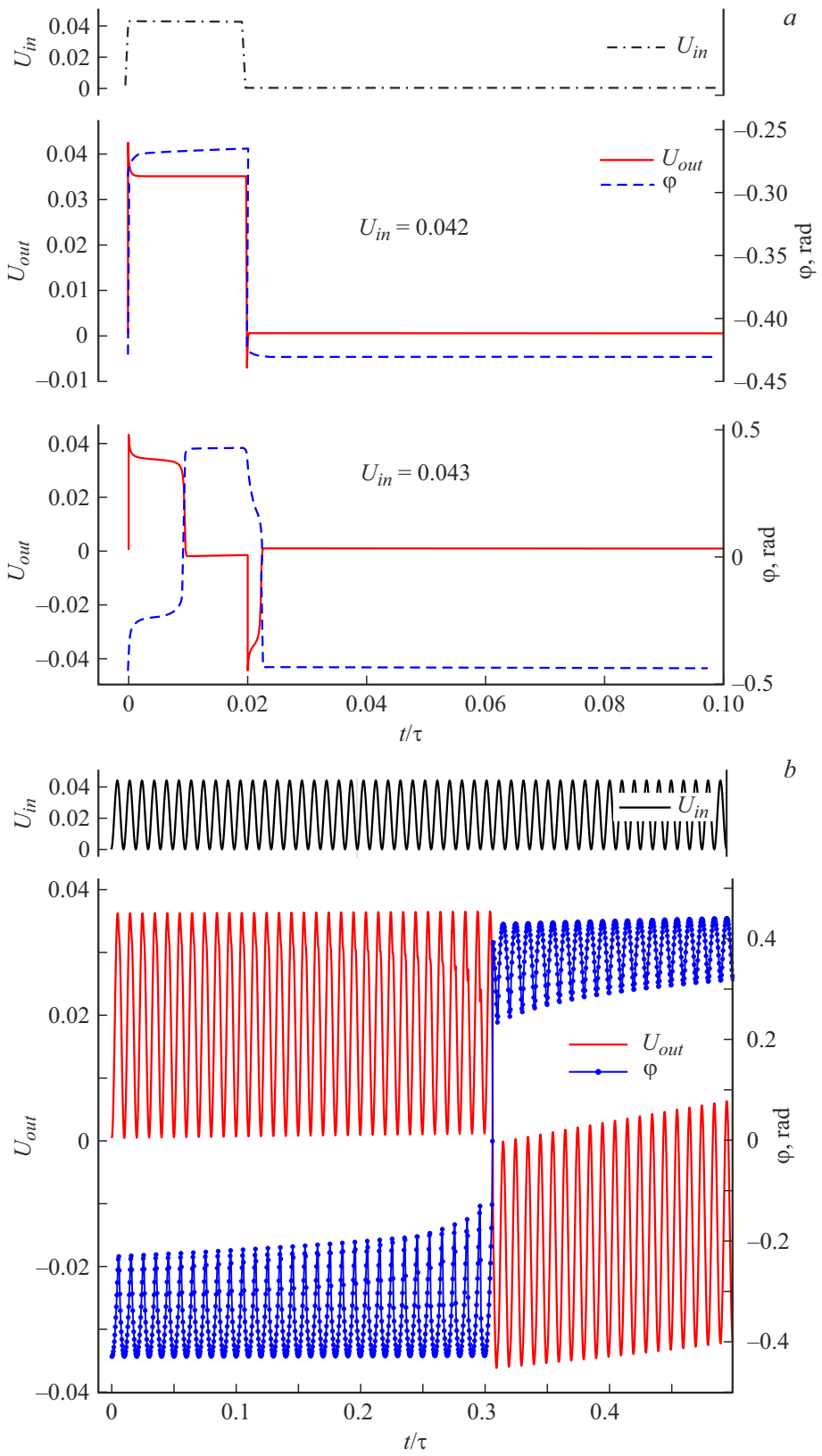

Figure 3. Pulsed transfer functions of the structure and time dependences of the magnetization orientation angle at $H = 1.05\,H_A$, $\varphi_0 = -0.43$. *a* — input pulses of short duration compared to the charge relaxation time (top panet), sub-threshold mode $U_{in} < 0.043$ (middle panel), post-threshold negative-voltage spike caused by the magnetization motion under the bistability conditions at $U_{in} = 0.043$ (bottom panel). *b* — input signal in the form of short pulses (top panel), time-threshold inversion of the magnetization direction and output voltage polarity (bottom panel).

transfer function presented in Fig. 2, *b* for $H = 1.05\,H_A$ ($\varphi_0 = -0.43$). The input signal increase to threshold level $U_{in} = 0.04\,H_A$ results in formation of a negative spike in the output voltage. The input signal switch-off turns the system to the equilibrium state.

In the case of pulsed input signals with characteristic times much shorter than the charge relaxation times, which is illustrated in Fig. 3, *a*, the output voltage increases monotonically with increasing input voltage and has a magnitude close to latter's (middle curve). At the end of the input pulse, the system returns to its initial state. When the threshold input voltage is exceeded ($U_{in} > 0.04$), a negative output voltage spike gets formed, after which the system also restores its initial state (lower curve in Fig. 3, *a*).

When the system is excited by a sequence of short pulses approximated by a periodical function, it exhibits the cumulative effect and threshold switching at the times comparable with those of charge relaxation (Fig. 3, *b*). In this case, the spin system irreversibly turns from one bistable state to another. The reverse transition may be achieved by inversion of the input pulse polarity.

The presented results demonstrate high functionality of nonlinear signal transformation with the aid of a straintronic multiferroic whose transfer function is being varied by controlling the magnetizing field without changing the device design.

Financial support

The study was supported by the RF Government grant № 075-15-2022-1131.

Conflict of interests

The authors declare that they have no conflict of interests.

References

[1] O. Deperlioglu, U. Kose, Comput. Electr. Eng., **37**, 392 (2011). DOI: 10.1016/j.compeleceng.2011.03.010
[2] Z. Li, X. Geng, J. Wang, F. Zhuge, Front. Neurosci., **15**, 717947 (2021). DOI: 10.3389/fnins.2021.717947
[3] A. Mehonic, A.J. Kenyon, Front. Neurosci., **10**, 57 (2016). DOI: 10.3389/fnins.2016.00057
[4] J. Woo, D. Lee, Y. Koo, H. Hwang, Microelectron. Eng., **182**, 42 (2017). DOI: 10.1016/j.mee.2017.09.001
[5] K. Kondo, J.Y. Choi, J.U. Baek, H.S. Jun, S. Jung, T.H. Shim, J.G. Park, J. Phys. D: Appl. Phys., **51**, 504002 (2018). DOI: 10.1088/1361-6463/aad592
[6] D.W. Kim, W.S. Yi, J.Y. Choi, K. Ashiba, J.U. Baek, H.S. Jun, J.J. Kim, J.G. Park, Front. Neurosci., **14**, 309 (2020). DOI: 10.3389/fnins.2020.00309
[7] A.A. Bukharaev, A.K. Zvezdin, A.P. Pyatakov, Yu.K. Fetisov, Phys. Usp., **61**, 1175 (2018). DOI: 10.3367/UFNe.2018.01.038279.
[8] Y. Dusch, N. Tiercelin, A. Klimov, S. Giordano, V. Preobrazhensky, P. Pernod, J. Appl. Phys., **113**, 17C719 (2013). DOI: 10.1063/1.4795440
[9] A. Klimov, N. Tiercelin, Y. Dusch, S. Giordano, T. Mathurin, P. Pernod, V. Preobrazhensky, A. Churbanov, S. Nikitov, Appl. Phys. Lett., **110**, 222401 (2017). DOI: 10.1063/1.4983717
[10] A.A. Klimov, N. Tiercelin, V.L. Preobrazhensky, A.S. Sigov, P. Pernod, Bull. Russ. Acad. Sci. Phys., **83**, 888 (2019). DOI: 10.3103/S1062873819070207.
[11] N. Tiercelin, V. Preobrazhensky, P. Pernod, Appl. Phys. Lett., **92**, 062904 (2008). DOI: 10.1063/1.2841656
[12] N. Tiercelin, Y. Dusch, S. Giordano, A. Klimov, V. Preobrazhensky, P. Pernod, in *Nanomagnetic and spintronic devices for energy-efficient memory and computing*, ed. by J. Atulasimha, S. Bandyopadhyay (John Wiley & Sons, Ltd., 2016), ch. 8. DOI: 10.1002/9781118869239.ch8
[13] V.L. Preobrazhensky, L.M. Krutyansky, N. Tiercelin, P. Pernod, Tech. Phys. Lett., **46**, 38 (2020). DOI: 10.1134/S1063785020010113.
[14] F. Wang, L. Luo, D. Zhou, X. Zhao, H. Luo, Appl. Phys. Lett., **90**, 212903 (2007). DOI: 10.1063/1.2743393
[15] A. Mazzamurro, Y. Dusch, P. Pernod, O. Bou Matar, A. Addad, A. Talbi, N. Tiercelin, Phys. Rev. Appl., **13**, 044001 (2020). DOI: 10.1103/PhysRevApplied.13.044001
[16] X. Liu, J. Fu, Optik, **206**, 164342 (2020). DOI: 10.1016/j.ijleo.2020.164342
[17] M. Takeuchi, T. Itoh, H. Nagasaka, Thin Solid Films, **51**, 83 (1978). DOI: 10.1016/0040-6090(78)90215-8

Translated by Solonitsyna Anna